Applied Physics Letters

RESEARCH ARTICLE | APRIL 22 2025

Stacking-, strain-engineering induced altermagnetism, multipiezo effect, and topological state in two-dimensional materials

Wei Xun ; Xin Liu ; Youdong Zhang ; Yin-Zhong Wu ; Ping Li

Appl. Phys. Lett. 126, 161903 (2025)
https://doi.org/10.1063/5.0267525

Applied Physics Letters ARTICLE pubs.aip.org/aip/apl

Stacking-, strain-engineering induced altermagnetism, multipiezo effect, and topological state in two-dimensional materials

Cite as: Appl. Phys. Lett. **126**, 161903 (2025); doi: 10.1063/5.0267525
Submitted: 24 February 2025 · Accepted: 11 April 2025 ·
Published Online: 22 April 2025

Wei Xun,[1] Xin Liu,[1] Youdong Zhang,[1,a)] Yin-Zhong Wu,[2] and Ping Li[3,4,5,a)]

AFFILIATIONS

[1]School of Electronic Engineering, Jiangsu Vocational College of Electronics and Information, Huaian 223003, China
[2]School of Physical Science and Technology, Suzhou University of Science and Technology, Suzhou 215009, China
[3]State Key Laboratory for Mechanical Behavior of Materials, Center for Spintronics and Quantum System, School of Materials Science and Engineering, Xi'an Jiaotong University, Xi'an, Shaanxi 710049, China
[4]State Key Laboratory for Surface Physics and Department of Physics, Fudan University, Shanghai 200433, China
[5]State Key Laboratory of Silicon and Advanced Semiconductor Materials, Zhejiang University, Hangzhou 310027, China

[a)]**Authors to whom correspondence should be addressed:** z.yd@163.com and pli@xjtu.edu.cn

ABSTRACT

Altermagnetism, a recently identified form of unconventional antiferromagnetism (AFM), enables the removal of spin degeneracy in the absence of net magnetization that provides a platform for the low power consumption and ultra-fast device applications. However, a little attention has been paid to the relationship between stacking, strain, and altermagnet, the multipiezo effect, and the topological state. Here, we propose a mechanism to realize the altermagnet, the multipiezo effect, and the topological state in two-dimensional (2D) materials by the stacking and strain engineering. Based on the analysis of symmetry, we find that the spin splitting feature related to the Ut, PTt, M_zUt, or M_zPTt symmetries in altermagnet multilayers. In addition, we find that the stacking engineering can effectively realize the transform from antiferromagnetism to altermagnetism and semiconductor to metal for the Janus bilayer V_2SeTeO. More interestingly, the strain not only induces an intriguing multipiezo effect, encompassing the piezovalley, piezomagnetism, and piezoelectric, but also achieves the abundant topological phase. Our findings offer a generalized direction for manipulating the spin splitting, valley polarization, and topological states, promoting practical application of valleytronic and spintronic devices based on two-dimensional altermagnets.

Altermagnetism, a type of collinear magnetism distinguished from antiferromagnetism (AFM) and ferromagnetism (FM), has garnered growing research interest in condensed matter physics.[1–8] It exhibits spin splitting similar to that of a ferromagnet, while it forms the AFM-like order with zero net magnetization. The spin splitting in altermagnets arises from the magnetic space group and is safeguarded by crystal symmetry.[1,2] Moreover, the spin dependent Fermi surface of altermagnet shows the planar or bulk d-wave, g-wave, or i-wave symmetry. These characteristics of altermagnetic materials can lead to a variety of unique physical properties, such as the anomalous Hall effect with a strength comparable to that of FM,[9] the staggered spin-momentum interaction,[10] the giant and tunneling magnetoresistance effect,[11] the theoretically predicted spin-splitter torque[12] and experimentally proved,[13,14] the piezomagnetism and C-paired spin-momentum locking,[15] the nontrivial superconductivity,[16,17] and the anti-Kramers nodal surfaces and unconventional magnetism.[18] Until now, it mainly focuses on the investigated unique physical properties of three-dimensional materials such as RuO_2,[5,9,14] MnTe,[4,19,20] $FeSb_2$,[18] and CrSb.[21–23] However, two-dimensional (2D) altermagnetism is rarely reported,[24–28] which is in urgent need of systematic investigation.

The layer degree of freedom offers a unique platform for enriching and tuning unique physical phenomena.[29–31] For example, the magic-angle graphene superlattices induce unconventional superconductivity.[32] Moreover, the interlayer coupling can tune the magnetic ground state.[30,33] In addition, the layer Hall effect can be realized by layer-dependent engineer in multiferroic lattice.[34] Furthermore, the topological phase transitions can be achieved by changing the interlayer coupling.[35] Therefore, what unique properties are induced by the layer degree of freedom in the altermagnets, which are worth

investigating. In addition, strain engineering also provides an opportunity to investigate physics.[36–39] Under mechanical strain, the 2D materials show intriguing responses, including topological phase transition,[36–38,40] piezoelectricity,[41] and piezomagnetism.[42,43] The topological phase transition is tuned by strain that is the most common approach.[36–38,40] Piezoelectricity, a well-known electromechanical coupling phenomenon, enables the generation of voltage in response to mechanical strain.[41] In addition, piezomagnetism is only observed in certain AFM crystals, where external strain can induce a net magnetization.[42,43] It is worth noting that the valley has been proposed as the third degree of freedom beyond the electron's charge and spin.[44–50] Whether the strain can achieve piezovalley phenomenon?

In this work, we propose a mechanism to altermagnet, the multipiezo effect, and the topological state in 2D materials by the stacking and strain engineering. First, we prove the spin-layer coupling effect in bilayer V_2SeTeO. Then, we find that the stacking configuration not only realizes the transform from AFM to altermagnet but also accompanies the transition from semiconductor to metal. Moreover, a unique multipiezo effect, encompassing the piezovalley, piezomagnetism, and piezoelectric, can be achieved in bilayer V_2SeTeO. Noted that these two responses are independent of each other, which is different from magnetoelectric coupling. Finally, the Se-Te interface bilayer V_2SeTeO exhibits nodal loop under the 0%−3% uniaxial strain and the 0%−2% biaxial strain, while it forms the Weyl points at near X and Y points under the further increased compressive strain. In addition, the Se-Se/Te-Te interface bilayer V_2SeTeO becomes Dirac semimetal under the uniaxial/biaxial compressive strain of less than 2%. Our discovery of enriched physical properties in bilayer V_2SeTeO offers a platform for designing advanced multifunctional valleytronic and spintronic devices.

The structure optimization, magnetic, and electronic properties are employed the Vienna *Abinitio* Simulation Package (VASP) based on the framework of the density functional theory (DFT).[51–53] The generalized gradient approximation (GGA) with the Perdew-Burke-Ernzerhof (PBE) is implemented to describe the exchange-correlation energy.[54] The plane wave basis with a kinetic energy cutoff is set to be 600 eV. The $21 \times 21 \times 1\Gamma$-centered k meshes of Brillouin zone are used. A vacuum of 30 Å is added along the c-axis, to avoid the interaction between the sheet and its periodic images. The total energy and force convergence criterion are set to be −0.005 eV/Å and 10^{-8} eV, respectively. To describe strongly correlated 3d electrons of V,[55] the GGA + U method is applied with the Coulomb repulsion U value of 4.0 eV. The zero damping DFT-D3 method of Grimme is considered for van der Waals (vdW) correction in bilayer V_2SeTeO.[42] For all bilayer V_2SeTeO structures, we optimized the atomic positions and layer spacing. We chose the V-*d* orbit and Se-, Te-, O-*p* orbits to fit the Wannier function. The maximally localized Wannier functions (MLWFs) are performed to construct an effective tight-binding Hamiltonian to investigate the topological properties by Wannier90 and WannierTools software package.[56–58]

As shown in Fig. 1(a), it exhibits the crystal structure of monolayer Janus V_2SeTeO, which is a sandwich structure with three atomic layers. The plane formed by V and O atoms is sandwiched by Se and Te planes. The monolayer V_2SeTeO shows a tetragonal lattice structure with the space group of P4 mm and Te point group of C_{4v}. The calculated lattice constant is 3.93 Å for monolayer V_2SeTeO, while the bond length of V-Se and V-Te is 2.58 and 2.79 Å, respectively. We determine the magnetic ground state of monolayer V_2SeTeO by comparing the total energies of two typical magnetic configurations, including FM and AFM states. The AFM configuration energy is 394.39 meV lower than FM configuration, which indicates that the AFM state is the magnetic ground state. However, from the spin charge density of Fig. 1(e), it is not a normal AFM. The two V atoms, which possess opposite spin orientations, are connected by the M_{xy} mirror symmetry. This type of AFM phase is named as altermagnetism. Moreover, we calculate the band structure under the Coulomb repulsion U 1–5 eV, as shown in Fig. S1. When the U value is less than 1.5 eV, monolayer V_2SeTeO is metallic. Continuing to increase the U value to the U value to 2–4 eV, the system becomes a semi-metallic. When the $U > 4$ eV, the bandgap will open at X and Y points. We have added discussion in the revised manuscript.

Here, as shown in Figs. 1(b)–1(d), we consider three stacking orders bilayer V_2SeTeO, including the upper layer shifted the lower layer formed Se-Te interface bilayer V_2SeTeO; the upper layer reversed by the M_z mirror symmetry operation regarding the lower layer formed Se-Se and Te-Te interface bilayer V_2SeTeO. It is worth noting that the Se-Se and Te-Te interface bilayer V_2SeTeO have the space inversion symmetry (P), while breaks the P symmetry for Se-Te interface bilayer V_2SeTeO. Moreover, as shown in Figs. 1(f)–1(h), it can be clearly observed that the Se-Te forms an asymmetric charge transfer, while the strictly symmetric charge transfer is formed in Se-Se and Te-Te interfaces. It indicates that the Se-Te interface bilayer V_2SeTeO

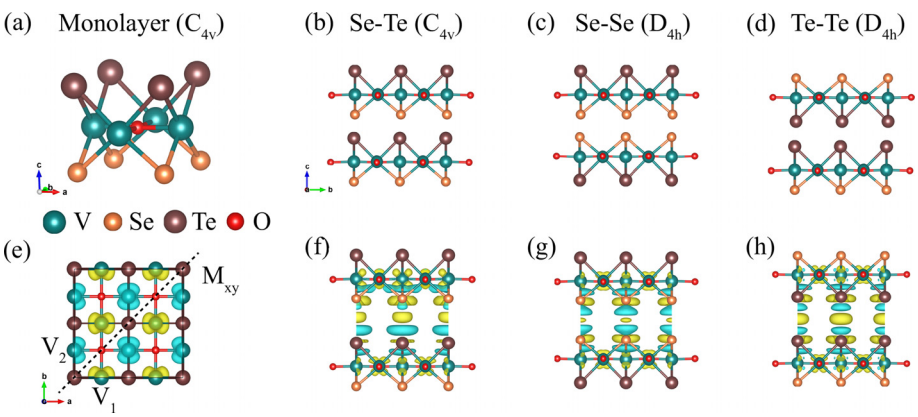

FIG. 1. (a) The side view of the crystal structure for monolayer V_2SeTeO. (b)–(d) The side view of bilayer V_2SeTeO, (b) Se-Te interface, (c) Se-Se interface, and (d) Te-Te interface. (e) Spin charge density of monolayer V_2SeTeO. (f)–(h) The differential charge density of bilayer V_2SeTeO, (f) Se-Te interface, (g) Se-Se interface, and (h) Te-Te interface. The yellow and light blue areas denote gain and loss electrons, respectively.

breaks the combination of time-reversal (T) and P symmetry (PT), while the Se-Se and Te-Te interface bilayer V_2SeTeO possess the PT symmetry.

In the AFM system, the energy eigenvalues $E_\uparrow(\mathbf{k})$ and $E_\downarrow(\mathbf{k})$ are connected, leading to the formation of fully spin-compensated bands. This phenomenon arises from the PT symmetry enabled by the two sublattices with opposite spins.[59] The P operation only reverses the vector k to generate $P\ E_\uparrow(k) = E_\uparrow(-k)$, and the T operation reverses both k and spin to generate $T\ E_\uparrow(k) = E_\downarrow(-k)$. Therefore, the PT symmetry guarantees that $E_\uparrow(k) = PT\ E_\uparrow(k) = E_\downarrow(k)$, leading to spin degenerate bands for the two spin components with opposite orientations in the k space. In addition, the translation operation (t) satisfies $t\ E_\uparrow(k) = E_\uparrow(k)$. Correspondingly, the energy eigenvalue exists $PTt\ E_\uparrow(k) = E_\uparrow(k)$ in the conventional AFM system. When the spin–orbit coupling (SOC) is ignored, the real space and spin space are completely decoupled. It will lead to $U\ E_\uparrow(k) = E_\uparrow(k)$, where U is the spin reversal operation. Noted that the spin reversal operation U is only suitable for collinear systems.

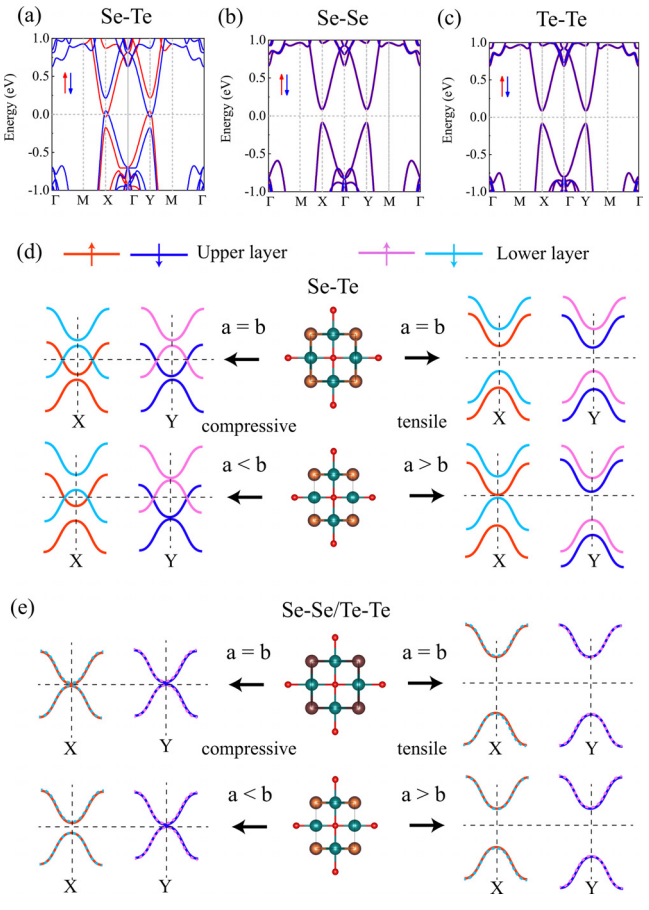

FIG. 2. (a)–(c) Spin-polarized band structure of (a) Se-Te interface, (b) Se-Se interface, and (c) Te-Te interface bilayer V_2SeTeO. The solid red and blue lines denote the spin up and spin down bands, respectively. (d) and (e) Schematic diagram of the piezovalley mechanism for (d) Se-Te interface and (e) Se-Se or Te-Te interface bilayer V_2SeTeO. The red, blue, magenta, and light blue lines represent spin up, spin down of the upper layer and spin up, spin down of the lower layer, respectively.

From the analysis discussed earlier, the existence of Ut or PTt symmetries in an altermagnet monolayer ensures the spin degeneracy. Due to the lack of an out-of-plane wave vector k in the low-dimensional system, the energy eigenvalues stay unchanged under the planar mirror symmetry M_z, satisfying $M_zE_\uparrow(k) = E_\uparrow(k)$. Therefore, when opposite spin sublattices are linked by Ut, PTt, M_zUt, or M_zPTt symmetries, the spin eigenvalues are completely degenerate at any wave vector k in the low-dimensional system.[2,60–63] In addition, the diagonal mirror symmetry M_Φ protects the valley degeneracy in the tetragonal structure, indicating that significant valley polarization can be realized through uniaxial strain, which breaks the lattice symmetry.

We propose that layertronics engineered by breaking specific symmetries can effectively control layer-spin locking and valley-contrasting properties, a concept that can be broadly applied to various 2D altermagnetic bilayers. Here, we investigate three typical Janus V_2SeTeO stacking structures. The Se-Se and Te-Te interface bilayer V_2SeTeO possess M_z and P symmetries, while the Se-Te interface bilayer V_2SeTeO breaks M_z and P symmetries. Therefore, PTt and M_zUt symmetries are broken for the Se-Te interface bilayer V_2SeTeO. As shown in Fig. 2(a), the spin degeneracy disappears, showing the characteristics of the altermagnetic band structure. Simultaneously, the spin up band of the upper layer and the spin down band of the lower layer cross at the Fermi level X point, while the spin down band of the upper layer and the spin up band of the lower layer cross at the Fermi level Y point (see Fig. S2). However, the sublattices of Se-Se and Te-Te interface bilayer V_2SeTeO are coupled by the PTt and M_zUt symmetries. Hence, as shown in Figs. 2(b) and 2(c), the band structures exhibit spin degeneracy. Meanwhile, as shown in Figs. S3 and S4, layer-resolved band structures are also degenerate. Moreover, we calculate the atom-resolved spin-polarized band structures for the Se-Te interface bilayer V_2SeTeO, as shown in Fig. S5. We find that the valley of the valence band mainly comes from Se and Te atoms, while the conduction band mainly comes from the V atom.

In general, the valley polarization exists in the broken P symmetry with ferroelectricity[64] or broken T symmetry with the SOC in the magnetic system.[65,66] However, the presence of valley polarization in bilayer V_2SeTeO relies on uniaxial strain to break the M_{xy} symmetry. This valley polarization can be understood as a response to strain and is named piezovalley. The physical mechanism of piezovalley is shown in Figs. 2(d) and 2(e). The valley polarization of bilayer V_2SeTeO is defined as the energy difference ΔV and ΔC between X and Y at the valence band maximum (VBM) and the conduction band minimum (CBM), $\Delta C(V) = E_{Xc(v)} - E_{Yc(v)}$. Figures 3(a) and S6(a) exhibit the evolution of valley polarizations and band gaps in the Se-Te interface bilayer V_2SeTeO under varying uniaxial strain. When the uniaxial strain is less than 2%, the Se-Te interface bilayer V_2SeTeO is in a metallic state. Continuing employing the uniaxial tensile strain to 2%, the Y point opens a gap, while the X point remains closed (see Fig. S7). We named it the half-valley metal. At the 5% uniaxial tensile strain, the valley splitting of VBM and CBM is up to −8.8 and 191.8 meV, respectively. In addition, it appears metallic under the biaxial strain of less than 1%, while it exhibits semiconductor at biaxial strains greater than 2%. As shown in Fig. S7, they all exhibit good altermagnetic signatures. These findings demonstrate that the Se-Te interface bilayer V_2SeTeO maintains an altermagnetic structure and achieves significantly enhanced piezovalley properties under strain.

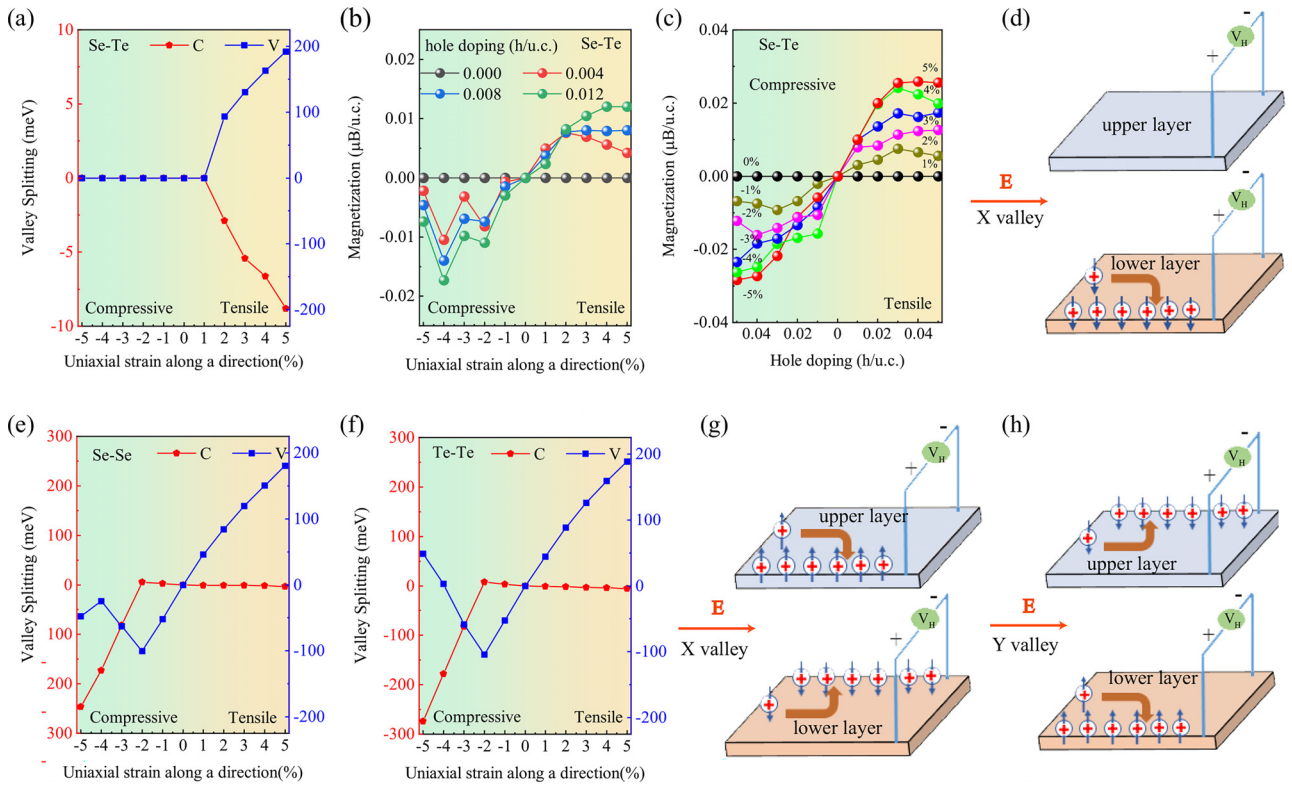

FIG. 3. (a) Valley splitting of Se-Te interface bilayer V_2SeTeO as a function of uniaxial strain along a direction. The valence and conduction bands are labeled V and C, respectively. (b) and (c) The net magnetization per unit cell as a function of hole-doping concentration. (d) Schematic diagram of spin-layer locked anomalous valley Hall effect in the hole-doped Se-Te interface bilayer V_2SeTeO at the X valley. The holes are denoted by the + symbol. Downward arrows show the spin down carriers. (e) and (f) Valley splitting of (e) Se-Se interface and (f) Te-Te interface bilayer V_2SeTeO as a function of uniaxial strain along a direction. The valence and conduction bands are labeled V and C, respectively. (h) and (i) Schematic diagram of valley layer-spin Hall effect for (h) X valley and (i) Y valley. The holes are shown by the + symbol. Upward and downward arrows represent the spin up and spin down carriers, respectively.

Strain-induced valley splitting in the Se-Te interface bilayer V_2SeTeO provides the effective approaches to generate net magnetization. The magnetism is determined by integrating the spin density within the energy range from negative infinity up to the Fermi level. The carrier doping can be effectively tuned the Fermi level cross only one valley, leading to the creation of net magnetic moments. The net magnetic moment is defined as $M = \int_{-\infty}^{E_f(n)} [\rho^{\uparrow}(\varepsilon) - \rho^{\downarrow}(\varepsilon)]\, dE$, where n, E_f, $\rho^{\uparrow(\downarrow)}$, and ε are the doping density, the doped Fermi level, the spin up (spin down) part of the density of states, and the external strain, respectively. In the absence of doping, the no net magnetization emerges in the strained Se-Te interface bilayer V_2SeTeO, which is consistent with the undoped band structures (see Fig. S7). At the certain doping concentration, the magnetization increases with uniaxial tensile strain, while it oscillates for uniaxial compressive strain. It is worth noting that the induced magnetization is opposite by uniaxial tensile and compressive strains. As shown in Figs. 3(b) and 3(c), under the small strain, the magnetization displays a linear response, which gradually saturates as the strain increases. The net magnetic moments generated by the piezomagnetic effect in the Se-Te interface bilayer V_2SeTeO are of the same order of magnitude as those previously reported in the monolayer V_2Se_2O and V_2SeTeO.[15,42] The characteristic altermagnetic structure of Se-Te interface bilayer V_2SeTeO, coupled with their low magnetocrystalline anisotropy, enables efficient manipulation of magnetic orientation and moments using the electric field and doping. With the hole-doping case, when the Fermi level is shifted between the X- and Y-valleys of the VBM, the spin down holes of X valley will be generated and accumulated on the left edge of the lower layer [see Fig. 3(d)]. Accordingly, the spin-layer locked anomalous valley Hall effect can be realized.

For the Se-Se and Te-Te interface bilayer V_2SeTeO, they exhibit the same pattern, since they all have *PT* symmetry. As shown in Figs. S9 and S11, the uniaxial compressive strain decreases the bandgap at the Y point, while the uniaxial tensile strain increases the bandgap at the Y point. When the uniaxial is less than −2%, both Se-Se and Te-Te interfaces become half-valley-metal. More interestingly, as shown in Figs. 3(e) and 3(f), the uniaxial strain can tune not only the magnitude but also the direction of valley polarization. It is worth noting that the uniaxial tensile strain can tune the VBM valley splitting to ∼200 meV, while the uniaxial compressive strain can regulate CBM valley splitting to ∼−300 meV. This has not been achieved in previous reports. In addition, the bandgap of X point, Y point, and total variation is shown in Figs. S6(b) and S6(c). On the contrary, the biaxial strain cannot realize valley splitting, but it can achieve semiconductor to metal transition (see Figs. S10 and S12). For the Se-Se and Te-Te

interfaces in the uniaxial tensile strain, as shown in Fig. 3(h), the spin up and spin down holes of X valley will generate and accumulate on the left edge of the upper layer and the right edge of the lower layer, respectively. When change from the uniaxial tensile strain to the uniaxial compressive strain, as shown in Fig. 3(i), the hole in the Y-valley will produce the exact opposite. We name the physical phenomenon the valley layer-spin Hall effect.

The strain realizes rich topological phase transitions. For the Se-Te interface bilayer V_2SeTeO, when the uniaxial compressive strain is in the 0%−−3% and the biaxial compressive strain is in the 0%−−2%, the band structure forms nodal loop near the Fermi level at both the X and Y points, which consists of different spin channels (see Figs. S7 and S8). Here, we exhibit the nodal loop of Se-Te interface bilayer V_2SeTeO under −1% biaxial strain in Fig. 4(a). Symmetry analysis uncovers that nodal loops near the X and Y points are protected by the M_z mirror symmetry. The nodal loops are situated in the xy plane, which remains invariant under the M_z mirror symmetry. When the compressive strain is further increased, the Weyl points are formed near X and Y points (see Figs. S7 and S8). For the Se-Se and Te-Te interface bilayer V_2SeTeO, when the uniaxial compressive strain surpasses −2%, the bandgap at the Y point is closed, while there is still a gap at X point, resulting in the formation of a Dirac point. It should be noted that the Dirac points are formed at both X and Y points, when the biaxial compressive strain is greater than −2%. Moreover, we calculated the edge state for the Te-Te interface bilayer V_2SeTeO. As shown in Fig. 4(b), one can clearly see an edge state connecting two Dirac points. It is worth noting that the Se-Te interface and Se-Se/Te-Te interface bilayer V_2SeTeO exhibit the different topological properties due to the unique crystal symmetries in these materials.

The piezoelectric effect, an intrinsic electromechanical coupling phenomenon in noncentrosymmetric materials, arises from strain or stress induced charge redistribution. It can result in the generation of electricity and formation of electric dipole moments. Therefore, as shown in Fig. 5, the Se-Te interface bilayer V_2SeTeO shows out-of-plane piezoelectricity due to the broken P and M_z symmetries. The second-rank piezoelectric stress tensor e_{ij} and strain tensor d_{ij} can be employed to describe the piezoelectric effect for 2D material. They can be obtained as the total of ionic and electronic contributions,

$$e_{ij} = \frac{\partial P_i}{\partial \varepsilon_j} = e_{ij}^{elc} + e_{ij}^{ion}, \tag{1}$$

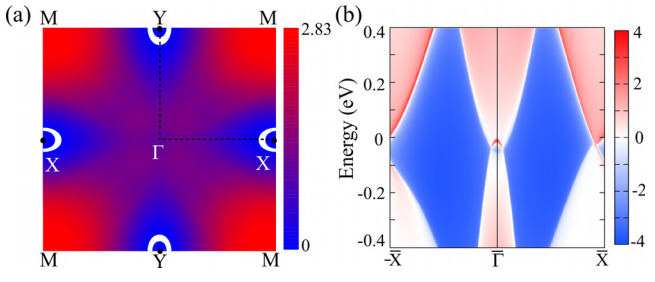

FIG. 4. (a) The nodal loop of Se-Te interface bilayer V_2SeTeO under −1% biaxial strain. The color map exhibits the local band gap at the cross of the two bands. (b) The edge state of Te-Te interface bilayer V_2SeTeO under −2% biaxial strain.

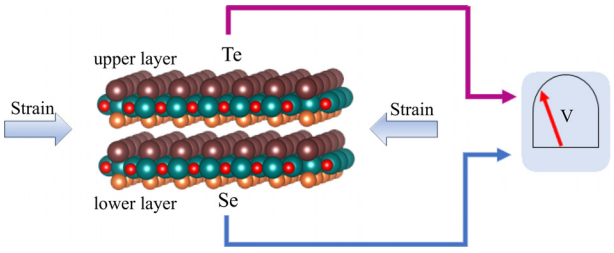

FIG. 5. Schematic diagram of generating an out-of-plane piezoelectric effect in Se-Te interface bilayer V_2SeTeO.

$$d_{ij} = \frac{\partial P_i}{\partial \sigma_j} = d_{ij}^{elc} + d_{ij}^{ion}, \tag{2}$$

where P_i, ε_j, and σ_j denote the polarization vectors, strains, and stresses, respectively. e_{ik} is related to d_{ik} by elastic tensor C_{jk}:

$$e_{ik} = d_{ij}C_{jk}. \tag{3}$$

By the Voigt notation, Eq. (3) with C_{4v} point group can be simplified as

$$\begin{pmatrix} 0 & 0 & 0 \\ 0 & 0 & 0 \\ e_{31} & e_{31} & 0 \end{pmatrix} = \begin{pmatrix} 0 & 0 & 0 \\ 0 & 0 & 0 \\ d_{31} & d_{31} & 0 \end{pmatrix} \begin{pmatrix} C_{11} & C_{12} & 0 \\ C_{12} & C_{11} & 0 \\ 0 & 0 & C_{66} \end{pmatrix}. \tag{4}$$

Hence, the out-of-plane piezoelectric coefficients d_{31} can be obtained as

$$d_{31} = \frac{e_{31}}{C_{11} + C_{12}}. \tag{5}$$

The calculated e_{31} is 0.765×10^{-10} C/m for the Se-Te interface bilayer V_2SeTeO, including the contributions of electrons 0.981×10^{-10} C/m and the contributions of ions -0.216×10^{-10} C/m. d_{31} is 0.57 pm/V obtained by formula Eq. (4). It is more than twice as large as that of monolayer V_2SeTeO.[42] The large vertical piezoelectric polarization is anticipated to enable multifunctional piezoelectric devices based on the Se-Te interface bilayer V_2SeTeO.

In conclusion, we propose a mechanism to manipulate the altermagnetic, multipiezo effect, and the topological state in two-dimensional materials. Based on the analysis of symmetry and first principles calculations, the mechanism is verified in Janus bilayer V_2SeTeO. By transforming the stacking configuration, one can effectively tune not only the transform from AFM to altermagnetism but also the phase transition from semiconductor to metal. More interestingly, the strain induces a unique multipiezo effect and the topological state. The uniaxial strain can tune the magnitude of valley splitting; simultaneously, the valley polarization direction can be changed. The net magnetic moments generated by the piezomagnetic effect in the Se-Te interface bilayer V_2SeTeO. In addition, the Se-Te interface bilayer V_2SeTeO shows nodal loop under the 0%−−3% uniaxial strain and the 0%−−2% biaxial strain while forms the Weyl points at near X and Y points under the further increased compressive strain. For the Se-Se/Te-Te interface bilayer V_2SeTeO, it becomes Dirac semimetal under the uniaxial/biaxial compressive strain of less than 2%. Our work provides a platform to investigate the altermagnetic, multipiezo effect, and the topological state in 2D altermagnets.

See the supplementary material for the additional results.

This work was supported by the National Natural Science Foundation of China (Grant Nos. 12404076, 12474238, and 12004295). P. Li also acknowledges supports from the China's Postdoctoral Science Foundation funded project (Grant No. 2022M722547), the Fundamental Research Funds for the Central Universities (No. xxj03202205), the Open Project of State Key Laboratory of Silicon and Advanced Semiconductor Materials (No. SKL2024-10), and the Open Project of State Key Laboratory of Surface Physics (No. KF2024_02). W. Xun also acknowledges supports from the Huai'an City Science and Technology Program Project (No. HAB2024069).

AUTHOR DECLARATIONS

Conflict of Interest

The authors have no conflicts to disclose.

Author Contributions

Wei Xun: Data curation (equal); Formal analysis (equal); Funding acquisition (equal); Investigation (equal). **Xin Liu:** Data curation (supporting). **Youdong Zhang:** Funding acquisition (equal); Resources (equal). **Yin-Zhong Wu:** Resources (equal). **Ping Li:** Conceptualization (equal); Data curation (equal); Formal analysis (equal); Funding acquisition (equal); Investigation (equal); Methodology (equal); Resources (equal); Software (equal); Supervision (equal); Writing – original draft (equal); Writing – review & editing (equal).

DATA AVAILABILITY

The data that support the findings of this study are available from the corresponding authors upon reasonable request.

REFERENCES

[1]L. Smejkal, J. Sinova, and T. Jungwirth, "Beyond conventional ferromagnetism and antiferromagnetism: A phase with nonrelativistic spin and crystal rotation symmetry," Phys. Rev. X **12**, 031042 (2022).
[2]L. Smejkal, J. Sinova, and T. Jungwirth, "Emerging research landscape of altermagnetism," Phys. Rev. X **12**, 040501 (2022).
[3]Y. P. Zhu, X. Chen, X. R. Liu, Y. Liu, P. Liu, H. Zha, G. Qu, C. Hong, J. Li, Z. Jiang, X. M. Ma, Y. J. Hao, M. Y. Zhu, W. Liu, M. Zeng, S. Jayaram, M. Lenger, J. Ding, S. Mo, K. Tanaka, M. Arita, Z. Liu, M. Ye, D. Shen, J. Wrachtrup, Y. Huang, R. H. He, S. Qiao, Q. Liu, and C. Liu, "Observation of plaid-like spin splitting in a noncoplanar antiferromagnet," Nature **626**, 523 (2024).
[4]J. Krempasky, L. Smejkal, S. W. DSouza, M. Hajlaoui, G. Springholz, K. Uhlirova, F. Alarab, P. C. Constantinou, V. Strocov, D. Usanov, W. R. Pudelko, R. G. Hernandez, A. B. Hellenes, Z. Jansa, H. Reichlova, Z. Soban, R. D. G. Betancourt, P. Wadley, J. Sinova, D. Kriegner, J. Minar, J. H. Dil, and T. Jungwirth, "Altermagnetic lifting of Kramers spin degeneracy," Nature **626**, 517 (2024).
[5]L. Smekal, A. Marmodoro, K. H. Ahn, R. G. Hernandez, I. Turek, S. Mankovsky, H. Ebert, S. W. D'Souza, O. Sipr, J. Sinova, and T. Jungwirth, "Chiral magnons in altermagnetic RuO_2," Phys. Rev. Lett. **131**, 256703 (2023).
[6]Y. Fang, J. Cano, and S. A. A. Ghorashi, "Quantum geometry induced nonlinear transport in altermagnets," Phys. Rev. Lett. **133**, 106701 (2024).
[7]S. B. Zhang, L. H. Hu, and T. Neupert, "Finite-momentum Cooper pairing in proximitized altermagnets," Nat. Commun. **15**, 1801 (2024).
[8]S. D. Guo, Y. Liu, J. Yu, and C. C. Liu, "Valley polarization in twisted altermagnetism," Phys. Rev. B **110**, L220402 (2024).
[9]Z. Feng, X. Zhou, L. Smejkal, L. Wu, Z. Zhu, H. Guo, R. G. Hernandez, X. Wang, H. Yan, P. Qin, X. Zhang, H. Wu, H. Chen, Z. Meng, L. Liu, Z. Xia, J. Sinova, T. Jungwirth, and Z. Liu, "An anomalous Hall effect in altermagnetic ruthenium dioxide," Nat. Electron. **5**, 735 (2022).
[10]H. Reichlova, R. L. Seeger, R. G. Hernandez, I. Kounta, R. Schlitz, D. Kriegner, P. Ritzinger, M. Lammel, M. Leiviska, V. Petricek, P. Dolezal, E. Schmoranzerova, A. Badura, A. Thomas, V. Baltz, L. Michez, J. Sinova, S. T. B. Goennenwein, T. Jungwirth, and L. Smejkal, "Macroscopic time reversal symmetry breaking by staggered spin-momentum interaction," arXiv:2012.15651 (2020).
[11]L. Smejkal, A. B. Hellenes, R. G. Hernandez, J. Sinova, and T. Jungwirth, "Giant and tunneling magnetoresistance in unconventional collinear antiferromagnets with nonrelativistic spin-momentum coupling," Phys. Rev. X **12**, 011028 (2022).
[12]R. G. Hernandez, L. Smejkal, K. Vyborny, Y. Yahagi, J. Sinova, T. Jungwirth, and J. Zelezny, "Efficient electrical spin splitter based on nonrelativistic collinear antiferromagnetism," Phys. Rev. Lett. **126**, 127701 (2021).
[13]S. Karube, T. Tanaka, D. Sugawara, N. Kadoguchi, M. Kohda, and J. Nitta, "Observation of spin-splitter torque in collinear antiferromagnetic RuO_2," Phys. Rev. Lett. **129**, 137201 (2022).
[14]H. Bai, L. Han, X. Y. Feng, Y. J. Zhou, R. X. Su, Q. Wang, L. Y. Liao, W. X. Zhu, X. Z. Chen, F. Pan, X. L. Fan, and C. Song, "Observation of spin splitting torque in a collinear antiferromagnet RuO_2," Phys. Rev. Lett. **128**, 197202 (2022).
[15]H. Y. Ma, M. Hu, N. Li, J. Liu, W. Yao, J. F. Jia, and J. Liu, "Multifunctional antiferromagnetic materials with giant piezomagnetism and noncollinear spin current," Nat. Commun. **12**, 2846 (2021).
[16]S. A. A. Ghorashi, T. L. Hughes, and J. Cano, "Altermagnetic routes to Majorana modes in zero net magnetization," Phys. Rev. Lett. **133**, 106601 (2024).
[17]H. G. Giil and J. Linder, "Superconductor-altermagnet memory functionality without stray fields," Phys. Rev. B **109**, 134511 (2024).
[18]I. I. Mazin, K. Koepernik, M. D. Johannes, R. G. Hernandez, and L. Smejkal, "Prediction of unconventional magnetism in doped $FeSb_2$," Proc. Natl. Acad. Sci. **118**, e2108924118 (2021).
[19]S. Lee, S. Lee, S. Jung, J. Jung, D. Kim, Y. Lee, B. Seok, J. Kim, B. G. Park, L. Smejkal, C. J. Kang, and C. Kim, "Broken Kramers degeneracy in altermagnetic MnTe," Phys. Rev. Lett. **132**, 036702 (2024).
[20]Z. Liu, M. Ozeki, S. Asai, S. Itoh, and T. Masuda, "Chiral split magnon in altermagnetic MnTe," Phys. Rev. Lett. **133**, 156702 (2024).
[21]J. Ding, Z. Jiang, X. Chen, Z. Tao, Z. Liu, T. Li, J. Liu, J. Sun, J. Cheng, J. Liu, Y. Yang, R. Zhang, L. Deng, W. Jing, Y. Huang, Y. Shi, M. Ye, S. Qiao, Y. Wang, Y. Guo, D. Feng, and D. Shen, "Large band splitting in g -wave altermagnet CrSb," Phys. Rev. Lett. **133**, 206401 (2024).
[22]M. Zeng, M. Y. Zhu, Y. P. Zhu, X. R. Liu, X. M. Ma, Y. J. Hao, P. Liu, G. Qu, Y. Yang, Z. Jiang, K. Yamagami, M. Arita, X. Zhang, T. H. Shao, Y. Dai, K. Shimada, Z. Liu, M. Ye, Y. Huang, Q. Liu, and C. Liu, "Observation of spin splitting in room-temperature metallic antiferromagnet CrSb," Adv. Sci. **11**, 2406529 (2024).
[23]G. Yang, Z. Li, S. Yang, J. Li, H. Zheng, W. Zhu, Z. Pan, Y. Xu, S. Cao, W. Zhao, A. Jana, J. Zhang, M. Ye, Y. Song, L. H. Hu, L. Yang, J. Fujii, I. Vobornik, M. Shi, H. Yuan, Y. Zhang, Y. Xu, and Y. Liu, "Three-dimensional mapping of the altermagnetic spin splitting in CrSb," Nat. Commun. **16**, 1442 (2025).
[24]S. Hayami, Y. Yanagi, and H. Kusunose, "Bottom-up design of spin-split and reshaped electronic band structures in antiferromagnets without spin-orbit coupling: Procedure on the basis of augmented multipoles," Phys. Rev. B **102**, 144441 (2020).
[25]S. D. Guo, X. S. Guo, K. Cheng, K. Wang, and Y. S. Ang, "Piezoelectric altermagnetism and spin-valley polarization in Janus monolayer Cr_2SO," Appl. Phys. Lett. **123**, 082401 (2023).
[26]Y. Liu, J. Yu, and C. C. Liu, "Twisted magnetic van der Waals bilayers: An ideal platform for altermagnetism," Phys. Rev. Lett. **133**, 206702 (2024).
[27]B. Pan, P. Zhou, P. Lyu, H. Xiao, X. Yang, and L. Sun, "General stacking theory for altermagnetism in bilayer systems," Phys. Rev. Lett. **133**, 166701 (2024).
[28]S. Zeng and Y. J. Zhao, "Bilayer stacking A-type altermagnet: A general approach to generating two-dimensional altermagnetism," Phys. Rev. B **110**, 174410 (2024).
[29]Y. Feng, Y. Dai, B. Huang, L. Kou, and Y. Ma, "Layer Hall effect in multiferroic two-dimensional materials," Nano Lett. **23**, 5367 (2023).

[30]W. Xun, C. Wu, H. Sun, W. Zhang, Y. Z. Wu, and P. Li, "Coexisting magnetism, ferroelectric, and ferrovalley multiferroic in stacking-dependent two-dimensional materials," Nano Lett. **24**, 3541 (2024).
[31]G. Yu, J. Ji, C. Xu, and H. J. Xiang, "Bilayer stacking ferrovalley materials without breaking time-reversal and spatial-inversion symmetry," Phys. Rev. B **109**, 075434 (2024).
[32]Y. Cao, V. Fatemi, S. Fang, K. Watanabe, T. Taniguchi, E. Kaxiras, and P. J. Herrero, "Unconventional superconductivity in magic-angle graphene superlattices," Nature **556**, 43 (2018).
[33]N. Sivadas, S. Okamoto, X. Xu, C. J. Fennie, and X. Xiao, "Stacking-dependent magnetism in bilayer CrI_3," Nano Lett. **18**, 7658 (2018).
[34]Y. Liu, Y. Feng, Y. Dai, B. Huang, and Y. Ma, "Engineering layertronics in two-dimensional ferromagnetic multiferroic lattice," Nano Lett. **24**, 3507 (2024).
[35]Y. Kim, P. Herlinger, P. Moon, M. Koshino, T. Taniguchi, K. Watanabe, and J. H. Smet, "Charge inversion and topological phase transition at a twist angle induced van hove singularity of bilayer graphene," Nano Lett. **16**, 5053 (2016).
[36]P. Li and T. Y. Cai, "Two-dimensional transition-metal oxides Mn_2O_3 realized the quantum anomalous Hall effect," J. Phys. Chem. C **124**, 12705 (2020).
[37]P. Li and T. Y. Cai, "Fully spin-polarized quadratic non-Dirac bands realized quantum anomalous Hall effect," Phys. Chem. Chem. Phys. **22**, 549 (2020).
[38]K. Wang, Y. Li, H. Mei, P. Li, and Z. X. Guo, "Quantum anomalous Hall and valley quantum anomalous Hall effects in two-dimensional d0 orbital XY monolayers," Phys. Rev. Mater. **6**, 044202 (2022).
[39]P. Li, C. Wu, C. Peng, M. Yang, and W. Xun, "Multifield tunable valley splitting in two-dimensional MXene Cr_2COOH," Phys. Rev. B **108**, 195424 (2023).
[40]J. Mutch, W. C. Chen, P. Went, T. Qian, I. Z. Wilson, A. Andreev, C. C. Chen, and J. H. Chu, "Evidence for a strain-tuned topological phase transition in $ZrTe_5$," Sci. Adv. **5**, eaav9771 (2019).
[41]M. N. Blonsky, H. L. Zhuang, A. K. Singh, and R. G. Hennig, "Ad initio prediction of piezoelectricity in two-dimensional materials," ACS Nano **9**, 9885 (2015).
[42]Y. Zhu, T. Chen, Y. Li, L. Qiao, X. Ma, C. Liu, T. Hu, H. Gao, and W. Ren, "Multipiezo effect in altermagnetic V_2SeTeO monolayer," Nano Lett. **24**, 472 (2024).
[43]Y. Jiang, X. Zhang, H. Bai, Y. Tian, B. Zhang, W. J. Gong, and X. Kong, "Strain-engineering spin-valley locking effect in altermagnetic monolayer with multipiezo properties," Appl. Phys. Lett. **126**, 053102 (2025).
[44]D. Xiao, W. Yao, and Q. Niu, "Valley-contrasting physics in graphene: Magnetic moment and topological transport," Phys. Rev. Lett. **99**, 236809 (2007).
[45]T. Cao, G. Wang, W. Han, H. Ye, C. Zhu, J. Shi, Q. Niu, P. Tan, E. Wang, B. Liu, and J. Feng, "Valley-selective circular dichroism of monolayer molybdenum disulphide," Nat. Commun. **3**, 887 (2012).
[46]P. Li, B. Liu, S. Chen, W. X. Zhang, and Z. X. Guo, "Progress on two-dimensional ferrovalley materials," Chin. Phys. B **33**, 017505 (2024).
[47]S. D. Guo, "Valley polarization in two-dimensional zero-net-magnetization magnets," Appl. Phys. Lett. **126**, 080502 (2025).
[48]Y. Wang, H. Sun, C. Wu, W. Zhang, S. D. Guo, Y. She, and P. Li, "Multifield tunable valley splitting and anomalous valley Hall effect in two-dimensional antiferromagnetic MnBr," Phys. Rev. B **111**, 085432 (2025).
[49]H. Sun, Y. Ren, C. Wu, P. Dong, W. Zhang, Y. Z. Wu, and P. Li, "Ferroelectric tuning of the valley polarized metal-semiconductor transition in $Mn_2P_2S_3Se_3$/Sc_2CO_2 van der Waals heterostructures and application to nonlinear Hall effect devices," Phys. Rev. Appl. **23**, 034032 (2025).
[50]C. Wu, H. Sun, P. Dong, Y. Z. Wu, and P. Li, "Coexisting triferroic and multiple types of valley polarization by structural phase transition in two-dimensional materials," Adv. Funct. Mater. **35**, 2501506 (2025).
[51]G. Kresse and J. Hafner, "Ab initio molecular dynamics for liquid metals," Phys. Rev. B **47**, 558 (1993).
[52]G. Kresse and J. Furthmuller, "Efficient iterative schemes for ab initio total-energy calculations using a plane-wave basis set," Phys. Rev. B **54**, 11169 (1996).
[53]G. Kresse and D. Joubert, "From ultrasoft pseudopotentials to the projector augmented-wave method," Phys. Rev. B **59**, 1758 (1999).
[54]J. P. Perdew, K. Burke, and M. Ernzerhof, "Generalized gradient approximation made simple," Phys. Rev. Lett. **77**, 3865 (1996).
[55]S. Grimme, J. Antony, S. Ehrlich, and H. Krieg, "A consistent and accurate ab initio parametrization of density functional dispersion correction (DFT-D) for the 94 elements H-Pu," J. Chem. Phys. **132**, 154104 (2010).
[56]A. A. Mostofi, J. R. Yates, Y. S. Lee, I. Souza, D. Vanderbilt, and N. Marzari, "wannier90: A tool for obtaining maximally-localised Wannier functions," Comput. Phys. Commun. **178**, 685 (2008).
[57]A. A. Mostofi, J. R. Yates, G. Pizzi, Y. S. Lee, I. Souza, D. Vanderbilt, and N. Marizari, "An updated version of wannier90: A tool for obtaining maximally-localised Wannier functions," Comput. Phys. Commun. **185**, 2309 (2014).
[58]Q. Wu, S. Zhang, H. F. Song, M. Troyer, and A. A. Soluyanov, "WannierTools: An open-source software package for novel topological materials," Comput. Phys. Commun. **224**, 405 (2018).
[59]S. Sheoran and S. Bhattacharya, "Multiple Zeeman-type hidden spin splittings in PT-symmetric layered antiferromagnets," Phys. Rev. B **109**, L020404 (2024).
[60]L. D. Yuan, Z. Wang, J. W. Luo, E. I. Rashaba, and A. Zunger, "Giant momentum-dependent spin splitting in centrosymmetric low-z antiferromagnets," Phys. Rev. B **102**, 014422 (2020).
[61]R. He, D. Wang, N. Luo, J. Zeng, K. Q. Chen, and L. M. Tang, "Nonrelativistic spin-momentum coupling in antiferromagnetic twisted bilayers," Phys. Rev. Lett. **130**, 046401 (2023).
[62]Y. Qi, J. Zhao, and H. Zeng, "Spin-layer coupling in two-dimensional altermagnetic bilayers with tunable spin and valley splitting properties," Phys. Rev. B **110**, 014442 (2024).
[63]J. Tian, J. Li, H. Liu, Y. Li, Z. Liu, L. Li, J. Li, G. Liu, and J. Shi, "Spin-layer coupling in an altermagnetic multilayer: A design principle for spintronics," Phys. Rev. B **111**, 035437 (2025).
[64]X. W. Shen, W. Y. Tong, S. J. Gong, and C. G. Duan, "Electrically tunable polarizer based on 2D orthorhombic ferrovalley materials," 2D Mater. **5**, 011001 (2017).
[65]W. Y. Tong, S. J. Gong, X. Wan, and C. G. Duan, "Concepts of ferrovalley material and anomalous valley Hall effect," Nat. Commun. **7**, 13612 (2016).
[66]P. Li, X. Yang, Q. S. Jiang, Y. Z. Wu, and W. Xun, "Built-in electric field and strain tunable valley-related multiple topological phase transitions in $VSiXN_4$ (X = C, Si, Ge, Sn, Pb) monolayers," Phys. Rev. Mater. **7**, 064002 (2023).